ADVANCED ENERGY MATERIALS
www.advenergymat.de

Electron Delocalization and Electrochemical Potential Distribution Phenomena in Faradaic Electrode Materials for Understanding Electrochemical Behavior

*Yachao Zhu, Siraprapha Deebansok, Jie Deng, Xuanze Wang, Thierry Brousse, Frédéric Favier, and Olivier Fontaine**

Electrochemical energy storage devices are built upon the foudations of batteries and supercapacitors. In the past decade, new pseudocapacitor-like electrodes are intensively developed to obtain superior energy storage performance. Pseudocapacitive matarials store charge through Faradaic processes, while the electrochemical signal remains like electrochemical double-layer capacitors (EDLCs). To address this controversy, an analytical model is introduced for evaluating the voltammograms of electrode materials. Given this, the work focuses on understanding the origin of the pseudocapacitive phenomena in the cyclic voltammetry (CV) electrochemical signal. Based on electron transfer mechanism and tunnelling effect within the atomic structure, pseudocapacitive matarials possess a high electron delocalization possibility related to the redox centers number and initiates the electrochemical potential distribution among neighboring redox sites, which is consequently observed in the electrochemical signal as the plateau feature in CV, like EDLC. First, the determination of the capacitive tendency of various electrode materials is proposed, which turns out to be relative to the redox centers number (n) and total charge (Z). Here, when this number is large, electron hopping will very likely happen. The developed model is versatile to predict rate/potential regimes for the maximum faradaic storage, and then well differentiates the pseudocapacitive and battery materials.

1. Introduction

The ever-growing global demand for energy underwent a sharp and sudden increase, leading to the expansion of energy storage technologies. Many of these storage technologies, most notably electrochemical energy storage, rely on redox processes.[1] The chemical composition of electrodes has been the topic of many studies to improve the performance of electrode materials in terms of energy and power densities.[2,3] Within this multiplicity of compositions, nanostructures, and properties, electrode materials are classified into two categories: non-Faradaic and Faradaic electrode materials. A non-Faradaic reaction points to one in which there is an absence of electron exchange across the electrode–electrolyte interface. In this case, charge storage occurs as a consequence of charging the electrochemical double layer at the electrode-solution

Y. Zhu, F. Favier
ICGM
Université de Montpellier
CNRS
Montpellier 34293, France

S. Deebansok, X. Wang, O. Fontaine
Molecular Electrochemistry for Energy Laboratory
School of Energy Science and Engineering
Vidyasirimedhi Institute of Science and Technology (VISTEC)
Rayong 21210, Thailand
E-mail: olivier.fontaine@vistec.ac.th

The ORCID identification number(s) for the author(s) of this article can be found under https://doi.org/10.1002/aenm.202304317

DOI: 10.1002/aenm.202304317

S. Deebansok
Advanced Institute for Materials Research (WPI-AIMR)
Tohoku University
Sendai 980-8577, Japan

S. Deebansok
Core Research Cluster for Materials Science (CRCMS)
Tohoku University
Sendai 980-8577, Japan

J. Deng
Institute for Advanced Study
Chengdu University
Chengdu 610106, China

T. Brousse
Nantes Université
CNRS
Institut des Matériaux de Nantes Jean Rouxel
IMN
2 rue de la Houssinière BP32229, Nantes cedex 3 44322, France

T. Brousse, F. Favier
Réseau sur le Stockage Electrochimique de l'Energie (RS2E)
CNRS FR 3459, 33 rue Saint Leu, Amiens Cedex 80039, France

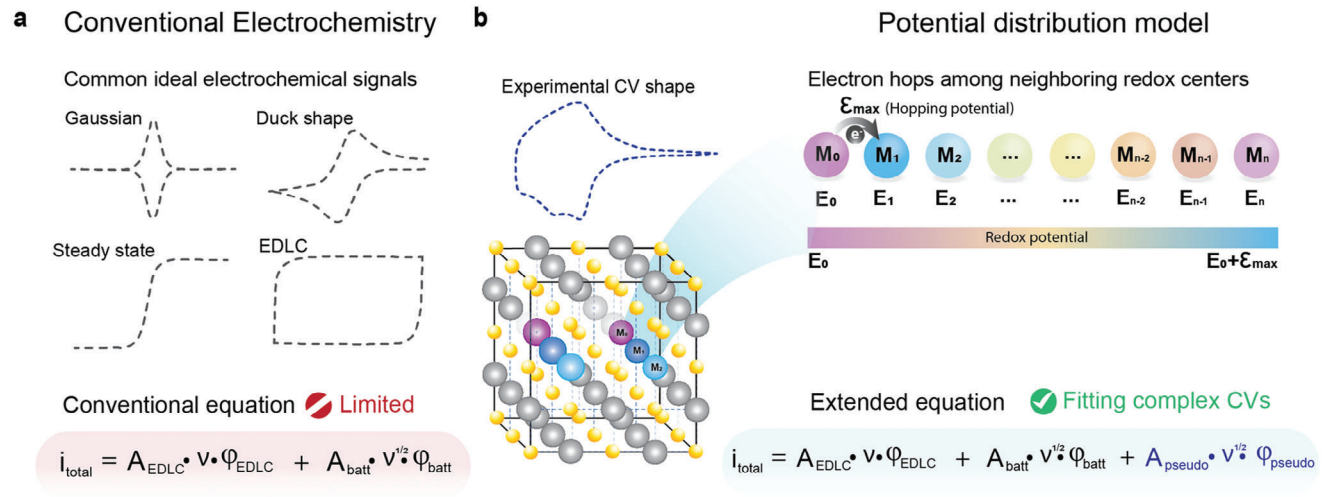

Figure 1. a) Conventional electrochemistry signals in ideal CVs with the conventional equation are limited to describe only simple CVs. b) Potential distribution model within the electrode material structure based on electron transfer between redox centers (M_0, M_1, ..., M_n) with the redox potentials respectively to each redox site, and our new extended equation for the total current leads to the first-time complex CV fitting.

interface. When Faradaic processes are engaged, however, electrons are transferred across the current collector to or from redox centers contained inside the electrode. Redox centers are buried in a solid phase, and the charging process thus involves the motion of counterions. The difference between these electrode materials is electrochemically detectable and is analyzed according to their physicochemical traits. Numerous characteristics are determined using a variety of methods, including electrochemical impedance spectroscopy and cyclic voltammetry (CV).[4,5] The CV technique has the advantage of varying the cell voltage (or potential, in a 3-electrode system) and observing the impact of these fluctuations on the cell dynamics (i.e., electron and ion transfer) while modulating the scan rate, that is, the time scale of the material studied.[6] While non-Faradaic electrode materials produce a box-shaped signal during CV measurements, Faradaic electrode materials present current peaks, indicating the potential value of their redox center.[7] However, Faradaic electrode materials are only seldom amenable to analysis through a perfect Gaussian peak signal, as idealized by the notion of immobilized redox centers (Figure S2a, Supporting Information). Similarly, a thorough examination of the $i = f(E)$ curves reveals that Gaussian peaks are not perfectly symmetrical (see Figure S2b, Supporting Information, for the ideal electrochemical response).

Surprisingly, there are no contemporary theories or formalist frameworks that make clear the story of faradaic materials well. To compound the issue, many more questions arise when addressing pseudocapacitive materials, which are characterized as Faradaic electrode materials that exhibit a box-shaped signature during a current-potential measurement (CV).[8] Two unsolved questions today are: first, how might it be possible to sign a Faradic phenomenon with a curve comparable to that of an electric double-layer capacitor (EDLC) material when the established signature must be Gaussian; second, which similarities and differences are present when comparing a Gaussian ideal material to a material with pseudocapacitive properties? The pseudocapacitor's box-shaped CV has been observed in a wide variety of transition metal oxides,[9] conducting polymers,[10] and other semiconducting redox materials. The mechanisms by which Faradaic reactions may exhibit quasi-rectangular capacitive electrochemical behavior remain unknown, and no cohesive model explaining the peculiarities of Faradaic electrode materials exists in the literature. Numerous studies, however, serve to demonstrate this pseudocapacitive behavior (Figure S1, Supporting Information).[2,4,11–44] This thus leads one to consider the possible reasons for a redox reaction, which is essentially a Faradaic occurrence, deviating so far from the ideal peak response (as illustrated in **Figure 1**).

Figure S3a, Supporting Information, illustrates the many and varied Faradaic electrode materials (i.e., those concerned with electron transfer), including both those used in pseudocapacitors, as well as those used in batteries. Regardless of which technical device is concerned, the electrode component, including its active material, stays constant. The active material stores charge through redox reactions involving the crystalline structure's redox center (as illustrated in Figure 1). As a result, this active material may be regarded as a matrix, with redox centers being connected by covalent bridges (Figure S3b, Supporting Information, e.g., oxygens) that lead these redox centers to interact. Naturally, the true nature of materials remains multifaceted including hierarchical porosity, multicrystalline structures, the presence of binders, conductive additives, and the percolation of highly conductive carbons near oxide particles.

In order to comprehend and rationalize the wide range of electrochemical reactions observed in Faradaic electrode materials (including pseudocapacitive materials), a three-step strategy is provided herein. The first step involves categorizing the relevant materials according to their n (number of redox centers per nm^3) and Z (electron included in crystalline structure) values. These parameters bring the effect of the n and Z values on the electrochemical signature to light. In the second step, the influence of n

and Z is then rationalized using a certain microscopic approach centered on electron transfer (i.e., the transition-state model). The third and final step, enabled by the first two in terms of creating a collection of parameters, makes use of these to simulate and compare theoretical and experimental electrochemical signal responses.

2. Results and Discussion

As stated before, there is no available model that combines the behavior of a battery with that of a pseudocapacitor currently. To complicate matters, these concepts are often separated into two distinct categories. This means that researchers find themselves without a coherent, universal method for analyzing and decoding electrochemical behavior (i.e., the shape of the cyclic voltammogram). A unified technique could be considered a significant step toward the future development of innovative, high-power batteries. We thus propose an integrated model, demonstrating that pseudocapacitive contributions indeed also exist in battery materials (Li-ion, Na-ion, and Mg-ion). CVs of batteries demonstrating their cell dynamics (electron and ion transport) are also shown to deviate significantly from the ideal signals published in the 1980s.

2.1. The Number of Redox Centers per nm^3 and the Z Value as Simple Markers for Distinguishing between Pseudocapacitive and Battery Materials

The primary goal is to be able to compare Faradaic electrode materials using three simple markers: i) n, the number of redox centers per nm^3 calculated as described in the Supporting Information (Section S5, Supporting Information), ii) Z, the number of electrons included in the crystalline structure, and iii) capacitive tendency, the ratio of peak current to plateau current is named pseudocapacitive percentage. The number of redox centers per cubic nanometer and the number of electrons per crystalline structure were determined for a series of lithium-ion batteries and pseudocapacitive materials. We compiled a list of 50 materials that are the most often used in electrochemical energy storage devices. Furthermore, we established a new parameter, the capacitive tendency. The capacitive tendency is the parameter to describe the electrochemical behavior of materials. This predictive model was published by some of us[45] using deep learning to classify electrochemical signals. The specific research involves using image classification to distinguish different curve shapes (rectangular shape and peak shape) that act on electrochemical signals, such as cyclic voltammetry, to connect electrochemical information (pseudocapacitor and batteries). When the capacitive tendency is close to 100%, the curve is more rectangular, and the material is more like a supercapacitor. When the capacitive tendency is close to 0%, the curve is more like a peak shape and the material is more like a battery. The capacitive tendency analyzes the shape of the voltammogram.

The capacitive tendency and capacitive contribution are not the same concept. Bruce Dunn et al.[46] proposed a model in 2007 that is proportional to current and scan rates, and used this model to describe the capacitive contribution and diffusion contribution in materials.[47–49] The capacitive contribution is different from the capacitive tendency proposed by some of us because the capacitive tendency is a metric to describe the shape of the material's signal curve and classify the material, rather than to calculate the proportion of capacitive contribution inside the material or provide the percentage of EDLC, pseudocapacitor or battery.

Alternatively, there is another simple way to calculate and express rectangular shape, which is called capacitive percentage, or simply $\%_{capa}$ (see Section S5 and Figure S5, Supporting Information). Equation (1) defines this pseudocapacitive percentage, but this result is just an approximate result. This one can only explain the general trend and the capacitive tendency is the result more accurate.

$$\%_{capa} = 100 - \frac{i_{max} - i_{min}}{i_{max}} \times 100 \quad (1)$$

where i_{max} is the maximum current and i_{min} is the relative minimum current taken after the faradaic contribution. **Figure 2** shows a heatmap of the capacitive tendency of all materials researched in the work.

This computation makes it possible to account for the nuances inherent in the voltammogram shapes as measured in the CV experiments. The $\%_{capa}$ is a useful indicator when it comes to anticipating the degree of charge delocalization. On the one hand, if the local minimum current is close to the maximum current, then the current is identical and the behavior displayed is rectangular (noting that the global resistance of the device is not taken into account in the calculation). This rectangular voltammogram represents the signature of so-called supercapacitive substances, be they EDLCs or pseudocapacitors. On the other hand, if the difference is significant, that is, the redox peak is highly prominent, then the behavior displayed is battery-like. Indeed, in order to accurately depict the electrochemical behavior of real-world voltammograms, calculating the $\%_{pseudo}$ thus allows for a simple categorization of the voltammogram shape, regardless of the material composition or lack thereof. The capacitive tendency is a graphical descriptor of a curve $i = f(E)$ that is independent of the usual material classification (battery, EDLC, pseudocapacitor).

The result of combining the redox center number per nm^3 with the electron number Z of the crystalline structure is shown in Figure 2. The cell count is based on the volume of each cell (see the CIF file, in Supporting Information), and the cell unit's Z' value indicates the number of material crystalline units repeated in one cell volume. In addition, the capacitive tendency is used for over 40 materials involved in the manuscript and compared with the $\%_{pseudo}$ results calculated from Equation (1), the complete result table is Table S4, Supporting Information.

In Figure 2 and Figures S7 and S8, Supporting Information, a scatter plot with a gradient of different colors denoting the capacitive tendency is used to position the 50 different materials.[5,50–96] Each of these materials is accompanied by voltammograms which were extracted from scientific publications. They were selected due to the fact that they are the most frequently applied materials in batteries and pseudocapacitors. For decades, these materials have been in constant evolution with the synthesis of new materials, the design of new structures, adjustments to their inner nature, and modifications to their morphology, all of which were geared toward maximizing

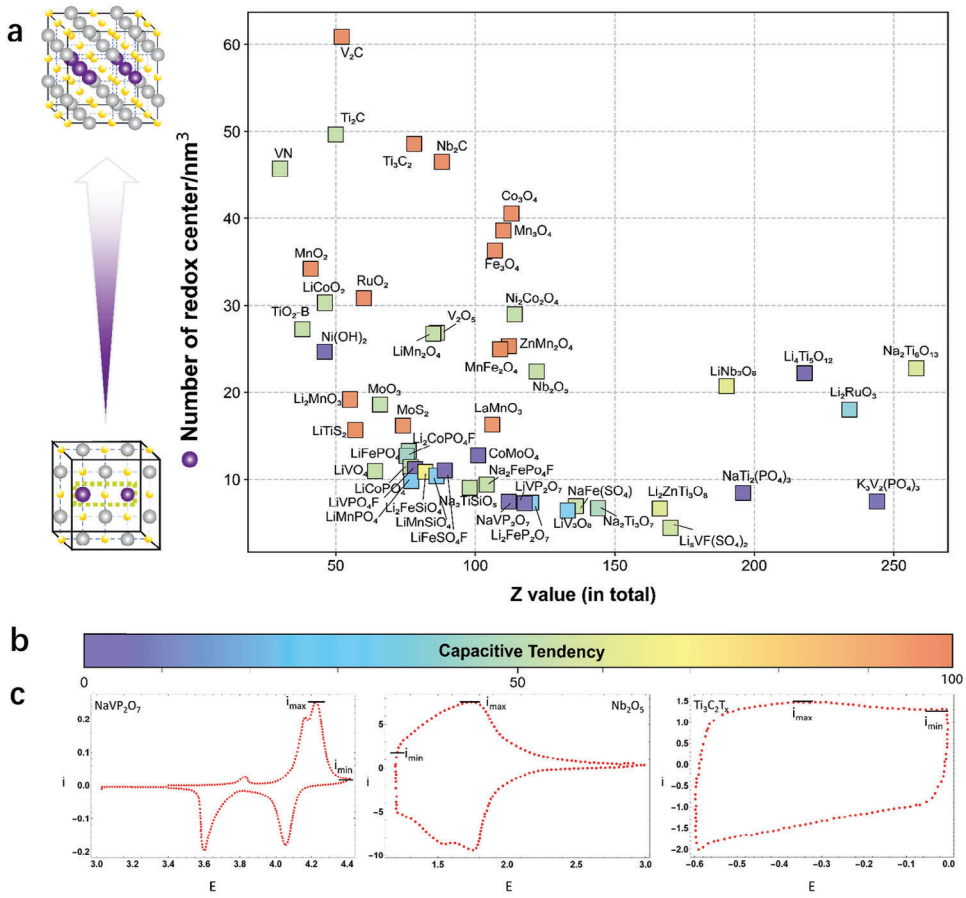

Figure 2. State-of-the-art in Faradaic electrode materials for batteries and pseudocapacitors. a) A list of materials classified according to capacitive tendency (ascribed to the color bar). The *y*-axis represents the number of redox centers per nm^3 and the *x*-axis represents the total number of electrons in the crystal structure. b) The qualitative color bar represents capacitive tendency. c) Typical voltammograms of the corresponding electrode material.

the capacitance/capacity to build advanced energy storage devices. As far as pseudocapacitive materials are concerned, RuO_2 stands out as one that underwent years of trials before finally shedding light on the mechanism of redox reactions in aqueous acidic electrolytes. This had to do with the valence change from Ru^{4+} to Ru^{3+}/Ru^{2+}, associated with proton insertion.[97,98] Another prominent one is MnO_2, which possesses a smooth ionic diffusion but displays limited electronic conductivity.[9] These two laid the groundwork for further research involving metal oxide-based Faradaic electrode materials such as TiO_2, Nb_2O_5, Co_3O_4, Mn_3O_4, and Fe_3O_4. In the case of Co_3O_4, it was found that morphological changes and size could lead to distinctive electrochemical behavior since when nano-sized it triggers a high-rate redox reaction. Aside from metal oxides, carbides and nitrides (e.g., vanadium nitride) also become the subject of research relating to redox reactions in pseudocapacitive materials. Among them, 2D MXenes, such as Ti_3C_2, Ti_2C, and V_2C, prevail due to their intriguing electronic conductivity and high-rate capability.[99,100] Numerous battery materials have been studied for use as anodes and cathodes in various battery cells. Current cathode materials that have already been commercialized include the well-known $LiCoO_2$ and $LiFePO_4$.[101] On the anode side, the most notable are $LiTi_4O_5$ and TiO_2.[102] It has been ascertained that battery materials exert redox reactions following phase changes after intercalating.[103–106] The materials selected for this study all serve to contribute to an overall picture of Faradaic electrode materials.

We observe an unmistakable trend whereby pseudocapacitive materials display a redox center density of between 20 and 60 per nm^3 and a Z value of between 0 and 120. In other words, a pseudocapacitive material has a large number of redox centers with a low number of electrons inside its crystalline structure. For battery materials, the number of redox centers is never greater than 30 per nm^3, while Z values can reach up to 140.

More specifically, MnO_2 and RuO_2 both show a capacitive tendency of close to 100% with a large number of redox centers per nm^3 and low Z values. Mn-based materials can be battery-type ones, such as Li_2MnO_3,[90] Li_2MnSiO_4,[96] and $LiMnPO_4$,[64] or pseudocapacitor-type ones such as MnO_2.[13] The same goes for Ti, with battery-type ones, such as $LiTiS_2$,[85] Na_2TiSiO_5,[59] $NaTi_2(PO_4)_3$,[83] $Li_4Ti_5O_{12}$,[71] and $Na_2Ti_6O_{13}$,[86] and pseudocapacitor-type ones such as Ti_2C[29] and Ti_3C_2.[11] Some materials are not a good fit for this simple classification, such as MoS_2[56] and MoO_3, which show around 17 redox centers per nm^3 and a Z value of around 70, all the while displaying

pseudocapacitive behavior. Co_3O_4, Mn_3O_4, and Fe_3O_4 exhibit large densities of redox centers together with high Z values, with capacitive tendency values of around 50%. 2D MXene materials, including Ti_3C_2 and V_2C, are pseudocapacitive materials with high redox center densities and low Z values. It should be noted that the choice of electrolyte probably has an impact on the capacitive tendency value. For example, for $Ti_3C_2T_x$-MXene,[29] the capacitive tendency value decreases from 80% to 50% (in KOH and H_2SO_4, respectively). V_2C-MXene[77] shows similar results. Concerning MnO_2 in an aqueous medium, the electrochemical reversibility can be highly impacted depending on the pH. This can be explained by a confinement phenomenon, where a transition occurs from double-layer to Faradaic charge storage.[107] The electrochemical interface actually involves porous or layered cases instead of an ideal planar model. With increasing interface complexity, charge transfer improves between an electrolyte ion and the host regarding the extent of ion desolvation and confinement. When K^+ intercalates in birnessite metal oxide, the K^+ is still hydrated without desolvation between interlayers, which offers a weak ion-host interaction and reduced charge transfer.

We have demonstrated that identifying the density of redox centers, n, and the corresponding Z values is enough to accurately predict the material type and the global shape of the cyclic voltammogram and vice versa. For the greater part of the researchers working in the field of electrochemical energy storage materials, determining the n and Z parameters will thus be quite straightforward. However, it is worth noting that the type of salt and nature of the solvent used in the electrolyte may sometimes affect the electrochemical behavior, and therefore the shape of the voltammogram.

To summarize, the capacitive tendency, and consequently the shape of the voltammogram, is chiefly governed by: 1) the number of redox centers per nm^3, and 2) the Z value of the crystalline structure, bearing in mind that 3) the nature of the electrolyte may have a certain effect on the result. It is then necessary to correlate these pieces of information within a model that explains why these three parameters affect the voltammogram signal. To this end, it is necessary to understand the impact that the proximity of the density of redox centers, n, has on the electron moving through the Faradaic electrode material.

2.2. Electron Movement as a Cause of Redox Potential Distribution

The initial Faradaic oxidative reactions that generate charges in the material are likely connected to ionic mobility, independently of the pseudocapacitive or battery-like behavior of the considered material. Therefore, the fundamental process of electron injection into a redox center remains a redox reaction, which is a Faradaic phenomenon. However, the spatial organization and density of the redox centers in battery and pseudocapacitive materials can produce quite a different outcome. The density of redox centers has a direct impact on the probability of an electron jumping from one redox center to another. Pseudocapacitive materials exhibit a large number of redox centers per nm^3, with a total exceeding 30. Following a charge injection (or extraction), the charge distribution then creates a distribution of redox potentials (as demonstrated in the following section). To explore this effect, we will first demonstrate that the probability of transferring an electron between two redox centers is greater when n is large and Z is small. In a subsequent step, we will show that an electron exchanged between two redox centers has an effect on the potential of neighboring centers.

To understand the possibility of an electron exchange between two redox centers, the probability of an electron hopping from one redox center to another may be expressed as the product of three separate probabilities. The first probability is equivalent to the chances of the electron encountering a neighboring redox center (noting that a defect in the crystalline structure will reduce this probability). The second probability is that a phonon (the vibration of a crystal lattice) causes the local distortion necessary for the temporary equalization of donor and acceptor levels (**Figure 3a**). The third probability is that tunneling occurs (Figure 3b), which is exponentially dependent upon the distance between the two considered redox centers.

According to this formalism, the greater the density of redox centers, the greater the probability of the electron being delocalized. This is consistent with the fact that a pseudocapacitive material has a large number of redox centers per nm^3, so the probability of charge delocalization is non-zero. It is worth noting that in the preliminary reports about the redox behavior of RuO_2, Trasatti et al.[108] emphasized this fact from the very start, stating, with respect to the metal cores, that the "*Me-Me* distance and the radius of the cation in these oxides are such that overlap of the inner d orbitals is possible, and the d electrons in the d bands are responsible for the metallic conduction", referring to Marcus studies on electron transfer to substantiate this remark.[109]

One particular "chemical" description of the proximity of the redox center may be investigated as a reaction comprising electron hopping. There are two alternatives when an electron is injected into a redox center: 1) The injected electron is restricted to the vicinity of the redox center (i.e., it is localized), or 2) the electron jumps to the nearest neighbor. After that, the charge is partially delocalized. This viewpoint is comparable to that of adiabatic versus diabatic electron transfer.[110]

Now, the electron transfers or hops from one redox center to the neighboring one in the electrode material structure. The redox reaction can be transcribed, along with the associated ionic transfer (where A is the anion) with equilibrium constant with the equilibrium ($K_{hopping}$) as follows:

$$A \times M^{(a+1)+} + M^{(a-1)+} \underset{k_{-1}}{\overset{k_1}{\rightleftarrows}} \underbrace{M^{(a)+} + M^{(a)+}}_{A} \tag{2}$$

where a is the reaction activity of a certain state.

If $k_1 \gg k_{-1}$ ($K_{hopping} \gg 1$) then the probability of an electron exchange between 2 redox centers is high, and inversely, if $k_1 \ll k_{-1}$ ($K_{hopping} \ll 1$), then the probability of an electron exchange is low. According to this equation, the way in which the redox charge is shared is based on an equilibrium constant, $K_{hopping}$. This equilibrium constant can then be expressed as the difference

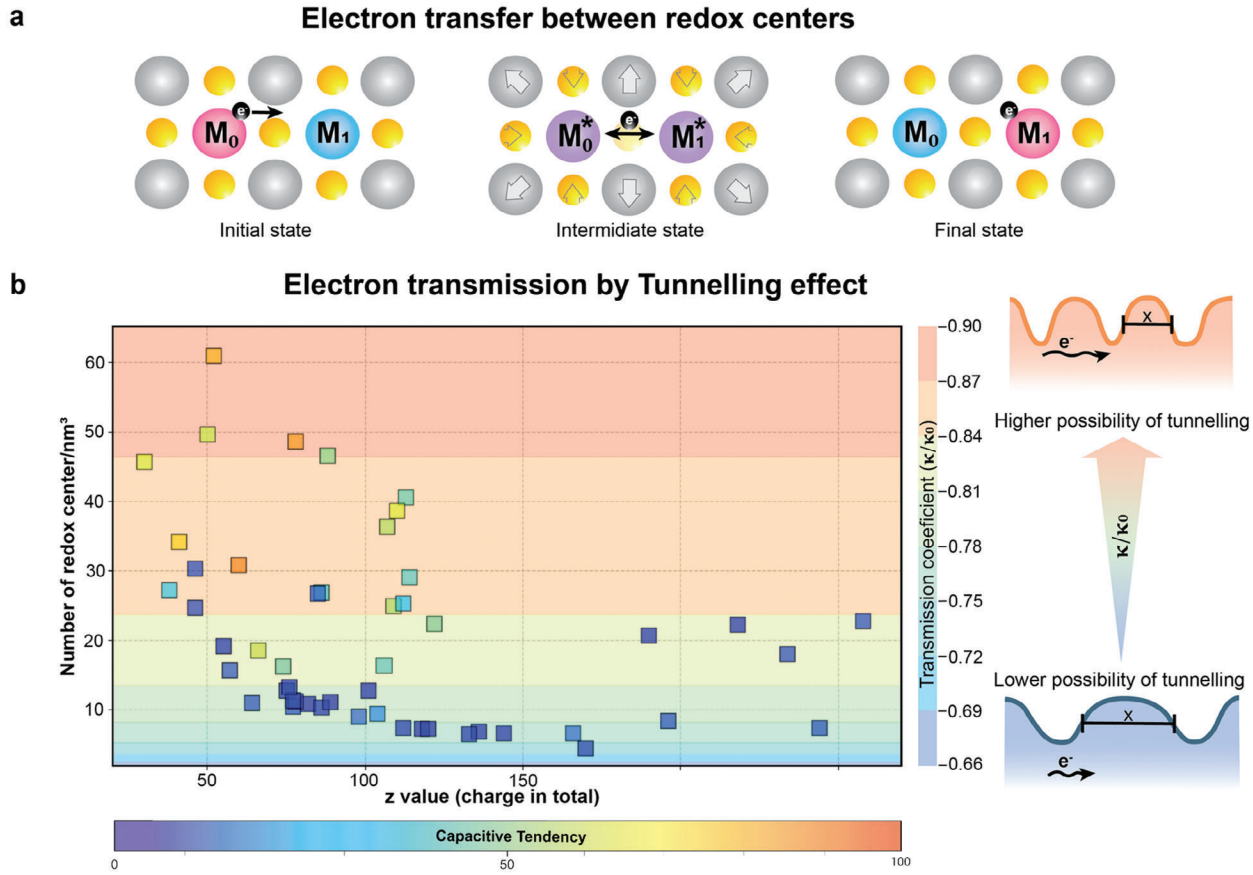

Figure 3. Electron transfer between two redox centers. a) The atomic changes associated with electron transfer for a solid structure. b) The electron transfer probability as a function of the number of redox centers (*y*-axis). The background color is with respect to the transmission coefficient of electron transfer according to the tunneling effect.

in redox potential required in order to oxidize both redox sites. E_0 is the potential to oxidize the first one, the so-called standard redox center and E_1 is the redox potential of the closest neighbor.

E_n corresponds to the redox potential of the umpteenth neighbor, then the umpteenth neighbor, $K_{hopping,n}$ is:

$$K_{hopping,n} = \exp\left[\frac{F \times (E_n - E_0)}{R \times T}\right] \quad (3)$$

where F is the Faraday constant (96 485 in C mol^{-1}), R is the gas constant (8.3145 J mol^{-1} K^{-1}), and T is the temperature (293.15 K).

The Equation (3) highlights two critical points: i) First, when two redox centers easily exchange electrons ($K_{hopping,1} \gg 1$), then the difference in potential between the two redox centers is quite large ($E_n - E_0 >> 0$). In other words, injecting a charge into one of the redox centers has an effect on the amount of work required to inject a charge into the redox center closest to it. ii) Second, the further away a neighbor is from the standard redox center, the less likely it is for them to share an electron. The potential distributes from the first redox center (M_0) to the nearest (M_1) and other neighboring redox centers (M_n) with hopping potential (ε).

n is the total number of potential hopping in the system, which corresponds to the number of neighbors nearest to the area where tunneling is likely to occur. ε_{max} and ε_{min} are the maximum and minimum potential differences between two redox centers as demonstrated in **Figure 4**.

The neighboring redox centers (M_i, when $i = 1, 2, 3, \ldots, n$ and i is the neighbor according to its position with respect to the standard redox center), the potential distributed is in descending order:

$$E_1 > E_2 \gg E_n > E_{n+1} \approx E_0 \quad (4)$$

Then

$$K_{hopping,1} > K_{hopping,2} > K_{hopping,3} \gg K_{hopping,n} \quad (5)$$

First, among n number of redox centers, started from M_0.

$$M_0, M_1, \ \ldots, M_{n-4}, M_{n-3}, M_{n-2}, M_{n-1}, M_n \quad (6)$$

At the farthest redox center (M_n), the lowest energy needed for the electron to jump, ε_{min}. By recurrence sequence, the hopping potential from the farthest to the nearest neighboring redox site is in ascending order:

$$n\varepsilon_{min}, \ \ldots, 5\varepsilon_{min}, 4\varepsilon_{min}, 3\varepsilon_{min}, 2\varepsilon_{min}, \varepsilon_{min} \quad (7)$$

So

$$E_{n-i} = E_0 + (i+1)\,\varepsilon_{min} \quad (8)$$

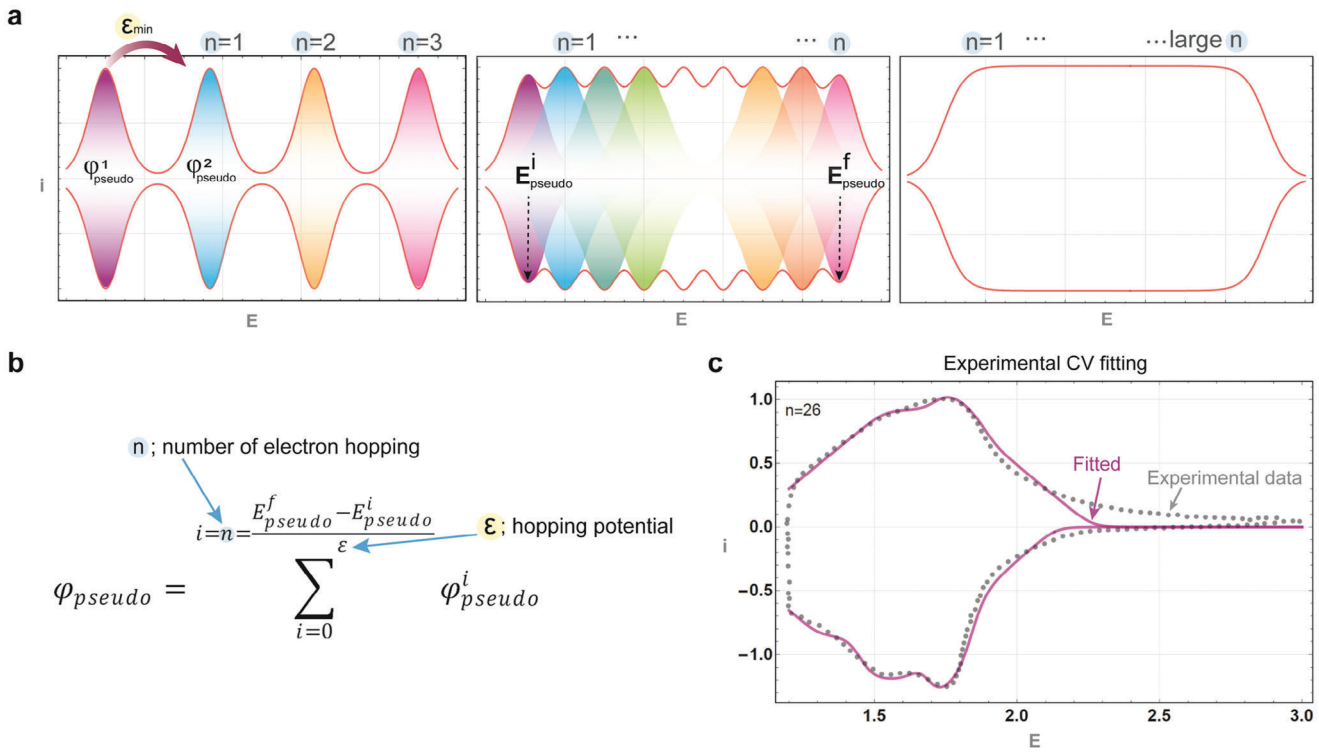

Figure 4. The formalism of the novel pseudocapacitor CV fitting method. a) Pseudocapacitor CV of various numbers of electron hopping (or the number of redox centers, n) and the potential distribution (or hopping potential, ε). b) The equation of pseudocapacitor signal. c) Experimental CV fitted by our formalism.

When

$$i = 1, 2, 3, \ldots, n \tag{9}$$

In this model of the redox potential distribution, there are three notable variables: ε_{max}, ε_{min} and n. So, ε_{max} is the work difference between the two nearest redox centers ($E_1 - E_0$). When a charge is injected into the standard redox center, its nearest neighbor has the most impacted electron affinity, so its redox potential is increased by a maximum jump (ε_{max}). Whereas the minimum potential jump corresponds to the furthest redox center influenced by the charge, noted by ε_{min}. Then n represents the number of neighbors influenced by the charge injection. Note that Equations (3) and (4) then become, for the general form:

$$K_{ET,i} = \exp\left[\frac{F \times \varepsilon_{max}}{i \times R \times T}\right] \tag{10}$$

and, for the nearest neighbor ($i = 1$)

$$K_{ET,1} = \exp\left[\frac{F \times \varepsilon_{max}}{R \times T}\right] \tag{11}$$

and, for the most distant neighbor ($i = n$)

$$K_{ET,n} = \exp\left[\frac{F \times \varepsilon_{min}}{R \times T}\right] \tag{12}$$

Figure S3, Supporting Information, illustrates the matrix model, including the redox potential distribution, using Equation (4). When redox centers are tightly packed together, the electron affinity decreases (i.e., it is more difficult to inject the electron into the nearest neighbor). This model involves a large redox potential distribution within the material.

A Faradaic electrode material is thus represented by the matrix, for which the continuous phase represents the overall charge in the crystalline structure and where the color of the redox centers is the distribution of redox potentials. Therefore, the proximity of the redox centers—high-density n—results in a broad redox potential distribution, as illustrated by the matrix model.

The rate constant, k_1, which is the kinetic constant of the electron transfer, is expressed by considering two rate-limiting steps. The first step is to consider that the electron transfer is sequential to the ion transfer. Therefore, k_1 will either be the electron transfer or the transfer of the counter-ion to be split. However, an alternative to this could be that the electron transfer is concomitant with the ion transfer so that the rate constant k_1 will reflect a new mathematical expression. Recently, Bazant et al. incorporated ion transfer effects into the kinetic theory of electron transfer.[111] The nature of the counterion can be varied such as Li^+, Na^+ Mg^{2+}, and Zn^{2+}.

Three phenomena influence the charge storage process in electrochemical energy storage materials: 1) the tunneling effect, 2) the chemical environment of the redox center, and 3) the effect of the counterion from the electrolyte. By analogy with the electron transfer in solution, therefore, a link in charge

processes exists. The crystalline structure, the counterions, and the distance between the redox centers all influence the ease with which charges can be delocalized. The effect of the counterion also deserves careful consideration, since the kinetics of electron exchange will be influenced by its probability of being shared or not, resulting in charge delocalization. Significantly, the charge delocalization induced by these three phenomena results in a redox potential distribution within the Faradaic electrode materials. This framework thus allows one to pinpoint the fundamental differences between a wide range of Faradaic electrode materials. Unexpectedly, however, battery materials display a partial charge distribution, implying that their charging mechanism must include a pseudocapacitive contribution. This last point is crucial, as these two types of materials are frequently pitted against each other in the scientific literature. Nonetheless, we demonstrate herein, for the first time, that by using our inclusive model one sees a strong connection between these two types of materials and can observe the source of this distinction. This is achieved by associating the redox potential distribution model with an experimentally exploitable electrochemical signal.

2.3. Using the Quantification of Redox Potential Distribution to Determine the Electrochemical Behavior of Faradaic Electrode Materials

Based on the probabilistic description of electron exchange through many redox centers, it is then necessary to create a model that incorporates the redox potential distributions of the electrochemical signals.

In this case, the signal would be the sum of the individual signals from n populations of redox centers, n being the variable developed in the previous section, that is, the number of neighbors impacted by the redox reaction of the so-called standard redox center. In a similar way to the EDLC current and the battery current, the current resulting from a pseudocapacitive contribution is expressed as:

$$\varphi_{\text{pseudo}} = \sum_{i=0}^{i=n=\frac{E^{f}_{\text{pseudo}}-E^{i}_{\text{pseudo}}}{\varepsilon}} \varphi^{i}_{\text{pseudo}} \tag{13}$$

The contribution of the neighbor i would then be similar to the mathematical expression of the pure battery current as follows:

$$\varphi^{i}_{\text{pseudo}} = \frac{R\times T}{2\times F\times G}\cdot e^{\frac{F}{R\times T}\cdot\left(E_{\text{apply}}-\left(E^{i}_{\text{pseudo}}+n\varepsilon\right)\right)}\left(\frac{e^{\frac{F\times G}{R\times T}}}{1+e^{\frac{F\times G_{\text{pseudo}}}{R\times T}}\cdot e^{\frac{F}{R\times T}\cdot\left(E_{\text{apply}}-\left(E^{i}_{\text{pseudo}}+n\varepsilon\right)\right)}}-\frac{e^{\frac{-F\times G}{R\times T}}}{1+e^{\frac{-F\times G}{R\times T}}\cdot e^{\frac{F}{R\times T}\cdot\left(E_{\text{apply}}-\left(E^{i}_{\text{pseudo}}+n\varepsilon\right)\right)}}\right) \tag{14}$$

where n is the number of potential hopping between redox centers (per nm^3), ε is the hopping potential (in V), E^{i}_{pseudo} is the standard redox potential of the pseudocapacitive current (in V), E^{f}_{pseudo} is the final potential of the pseudocapacitive current (in V), and $\varphi^{i}_{\text{pseudo}}$ is the neighboring pseudocapacitive current (dimensionless current). For the first time, herein we thus propose a homogeneous and universal formalism for simulating a voltammogram, irrespective of the origin of its redox dynamics, for all electrochemical energy storage materials, be they electrochemical double layer, purely battery-type or pseudocapacitive in nature. Moreover, via this formalism, we can show that all electrode materials possess a combination of these three contributions. However, the contribution of each of the components will then be more or less intense, depending on the value of the maximum current ($i^{\max}_{\text{EDLC}}$, $i^{\max}_{\text{pseudo}}$, $i^{\max}_{\text{batt}}$), that is:

$$i_{\text{tot}} = i^{\max}_{\text{EDLC}}\times\varphi_{\text{EDLC}} + i^{\max}_{\text{pseudo}}\times\varphi_{\text{pseudo}} + i^{\max}_{\text{batt}}\times\varphi_{\text{batt}} \tag{15}$$

Figure S11, Supporting Information, shows CV profiles of various electrochemical systems, including $i_{\text{peak}} + i_{\text{EDLC}}$, pure i_{pseudo}, $i_{\text{pseudo}} + i_{\text{EDLC}}$, and the contour plots of % pseudo of these systems related to the resistance and scan rate. These results were obtained by using the Wolfram Language with its Mathematica tool to plot the functions according to Equation (10), where $A_{\text{batt}} = A_{\text{EDLC}} = A_{\text{pseudo}} = 1$ was considered. First, the different current profiles of the first two models in Figure S11a,b, Supporting Information, with different values for R_s and ν, can be observed. These characteristics relate to different $\%_{\text{pseudo}}$ as indicated in the contour plot (Figure S11c, Supporting Information). One can clearly see that, even when increasing the scan rate, the $\%_{\text{pseudo}}$ still barely reaches 90% as a result of the peak current contribution. This result agrees with experimental observations (see Supporting Information). Second, the rectangular CV profile (Figure S11d,e, Supporting Information) is distorted by the presence of i_{EDLC} current with a large $R_s = 50\ \Omega$. Similarly, Figure S11f, Supporting Information, demonstrates $\%_{\text{pseudo}}$ as a function of the R_s and the scan rate for a pseudocapacitive current with the contribution of i_{EDLC}. It was found that the $\%_{\text{pseudo}}$ is high, even when increasing the scan rate. This result also agrees with experimental observations (Figures S13–S60, Supporting Information).

Figure 4a shows the proposed pseudocapacitor model where the redox peaks start to overlap with the number of electron hopping. The extended formalism from Equation (8) (as demonstrated in Figure 4b) was finally introduced into the total current with other current components (Equation (10)). Using this model, an experimental CV was well-fitted, as shown in Figure 4c. It was also found that, even in the battery materials, there is a certain pseudocapacitive contribution resulting from the distribution of the potential to the nearby redox centers when the number of redox centers per nm^3 is high, as presented in the corresponding matrix models with numerous redox centers (Figures S13–S60, Supporting Information).

The conventional method is to use the peak current to determine whether a device is a battery or a pseudocapacitor. While the peak current model is a good fit, the signal including all

potential ranges is incomplete. Moreover, the model proposed herein has shown a strong correlation between state-of-the-art experience and reliable theory. Besides, this proposed theory is based on equilibrium exchange between two redox centers, so it cannot be used to analyze the reversibility of the charge–discharge process.

3. Conclusion

Batteries and supercapacitors are both widely used electrochemical energy storage technologies. When it comes to batteries, redox processes display unusual electrochemical behavior, for which there is no clear explanation to date. Complicating matters further, no universal analytical formalism for assessing voltammograms has thus far been proposed. This article began by discussing the electrochemical properties of batteries and pseudocapacitive materials, as well as what sets them apart while focusing on electron transport pathways. We have shown that battery and pseudocapacitor materials, called Faradaic electrode materials, both exhibit strong electron delocalization resulting in large redox potential distributions due to tunneling and the polaron effect. Perhaps more significantly, battery materials display the same potential dispersion, albeit weaker. Faradaic electrode materials are very much in the scientific limelight of late, and our research serves to provide a link between them all, thereby culminating in a ground-breaking, all-inclusive model for assessing such materials.

Supporting Information

Supporting Information is available from the Wiley Online Library or from the author.

Conflict of Interest

The authors declare no conflict of interest.

Author Contributions

Y.Z. and S.D. contributed equally to this work. S.D. thanks Vistec for the financial support of the work during her position as assistant researcher. For S.D., the present work was fully done in Vistec, Thailand. O.F. developed all of the mathematical formalism. S.D. contributes to numerically coding the equations ordered by O.F.

Data Availability Statement

The data that support the findings of this study are available in the supplementary material of this article.

Keywords

battery, electron transfer, energy storage mechanism, molecular electrochemistry, supercapacitor

Received: December 13, 2023
Revised: March 5, 2024
Published online:

[1] P. Simon, Y. Gogotsi, *Nat. Mater.* **2020**, *19*, 1151.
[2] Y. Ando, M. Okubo, A. Yamada, M. Otani, *Adv. Funct. Mater.* **2020**, *30*, 2070312.
[3] V. Augustyn, P. Simon, B. Dunn, *Energy Environ. Sci.* **2014**, *7*, 1597.
[4] J. Come, V. Augustyn, J. W. Kim, P. Rozier, P.-L. Taberna, P. Gogotsi, J. W. Long, B. Dunn, P. Simon, *J. Electrochem. Soc.* **2014**, *161*, A718.
[5] J. Come, P. L. Taberna, S. Hamelet, C. Masquelier, P. Simon, *J. Electrochem. Soc.* **2011**, *158*, A1090.
[6] C. Costentin, T. R. Porter, J. M. Saveant, *ACS Appl. Mater. Interfaces* **2017**, *9*, 8649.
[7] C. Choi, D. S. Ashby, D. M. Butts, R. H. DeBlock, Q. Wei, J. Lau, B. Dunn, *Nat. Rev. Mater.* **2019**, *5*, 5.
[8] T. Brousse, D. Bélanger, J. W. Long, *J. Electrochem. Soc.* **2015**, *162*, A5185.
[9] M. Toupin, T. Brousse, D. Bélanger, *Chem. Mater.* **2004**, *16*, 3184.
[10] T. Liu, L. Finn, M. Yu, H. Wang, T. Zhai, X. Lu, Y. Tong, Y. Li, *Nano Lett.* **2014**, *14*, 2522.
[11] M. A. Aegerter, *Sol. Energy Mater. Sol. Cells* **2001**, *68*, 401.
[12] C. R. Arias, C. Debiemme-Chouvy, C. Gabrielli, C. Laberty-Robert, A. Pailleret, H. Perrot, O. Sel, *J. Phys. Chem. C* **2014**, *118*, 26551.
[13] D. Chen, D. Ding, X. Li, G. H. Waller, X. Xiong, M. A. El-Sayed, M. Liu, *Chem. Mater.* **2015**, *27*, 6608.
[14] M. I. M. Chigane, *J. Electrochem. Soc.* **2000**, *147*, 2246.
[15] S. Cong, Y. Tian, Q. Li, Z. Zhao, F. Geng, *Adv. Mater.* **2014**, *26*, 4260.
[16] K. Ganeshan, Y. K. Shin, N. C. Osti, Y. Sun, K. Prenger, M. Naguib, M. Tyagi, E. Mamontov, D. E. Jiang, A. C. T. van Duin, *ACS Appl. Mater. Interfaces* **2020**, *12*, 58378.
[17] N. Jabeen, Q. Xia, S. V. Savilov, S. M. Aldoshin, Y. Yu, H. Xia, *ACS Appl. Mater. Interfaces* **2016**, *8*, 33732.
[18] A. Jadon, S. Prabhudev, G. Buvat, S. G. Patnaik, M. Djafari-Rouhani, A. Estève, D. Guay, D. Pech, *ACS Appl. Energy Mater.* **2020**, *3*, 4144.
[19] X. Ji, K. Xu, C. Chen, B. Zhang, Y. Ruan, J. Liu, L. Miao, J. Jiang, *Phys. Chem. Chem. Phys.* **2016**, *18*, 4460.
[20] K. Juodkazis, J. Juodkazytė, V. Šukienė, A. Grigucevičienė, A. Selskis, *J. Solid State Electrochem.* **2007**, *12*, 1399.
[21] C. Y. Lee, A. M. Bond, *Langmuir* **2010**, *26*, 16155.
[22] M.-T. Lee, W.-T. Tsai, M.-J. Deng, H.-F. Cheng, I. W. Sun, J.-K. Chang, *J. Power Sources* **2010**, *195*, 919.
[23] Z. Y. Leong, H. Y. Yang, *ACS Appl. Mater. Interfaces* **2019**, *11*, 13176.
[24] Y. Liu, F. Zhou, V. Ozolins, *J. Phys. Chem. C* **2011**, *116*, 1450.
[25] A. Llordes, G. Garcia, J. Gazquez, D. J. Milliron, *Nature* **2013**, *500*, 323.
[26] M. R. Lukatskaya, S.-M. Bak, X. Yu, X.-Q. Yang, M. W. Barsoum, Y. Gogotsi, *Adv. Energy Mater.* **2015**, *5*, 1500589.
[27] N. Sakai, Y. Ebina, K. Takada, T. Sasaki, *J. Electrochem. Soc.* **2005**, *152*, E384.
[28] M. R. Scherer, L. Li, P. M. Cunha, O. A. Scherman, U. Steiner, *Adv. Mater.* **2012**, *24*, 1217.
[29] H. Shao, K. Xu, Y.-C. Wu, A. Iadecola, L. Liu, H. Ma, L. Qu, E. Raymundo-Piñero, J. Zhu, Z. Lin, P.-L. Taberna, P. Simon, *ACS Energy Lett.* **2020**, *5*, 2873.
[30] S. Sopčić, M. K. Roković, Z. Mandić, A. Róka, G. Inzelt, *Electrochim. Acta* **2011**, *56*, 3543.
[31] P. Sun, Z. Deng, P. Yang, X. Yu, Y. Chen, Z. Liang, H. Meng, W. Xie, S. Tan, W. Mai, *J. Mater. Chem. A* **2015**, *3*, 12076.
[32] Y. Tian, S. Cong, W. Su, H. Chen, Q. Li, F. Geng, Z. Zhao, *Nano Lett.* **2014**, *14*, 2150.
[33] E. Watanabe, H. Ushiyama, K. Yamashita, Y. Morikawa, D. Asakura, M. Okubo, A. Yamada, *J. Phys. Chem. C* **2017**, *121*, 18975.
[34] D. Wei, M. R. Scherer, C. Bower, P. Andrew, T. Ryhanen, U. Steiner, *Nano Lett.* **2012**, *12*, 1857.
[35] Q. Wei, J. Liu, W. Feng, J. Sheng, X. Tian, L. He, Q. An, L. Mai, *J. Mater. Chem. A* **2015**, *3*, 8070.

[36] T. E. Wojtek Dmowski, K. E. Swider-Lyons, C. T. Love, D. R. Rolison, *J. Phys. Chem. B* **2002**, *106*, 12677.
[37] Z. Xie, X. Jin, G. Chen, J. Xu, D. Chen, G. Shen, *Chem. Commun. (Cambridge, U. K.)* **2014**, *50*, 608.
[38] P. Yang, P. Sun, Z. Chai, L. Huang, X. Cai, S. Tan, J. Song, W. Mai, *Angew. Chem., Int. Ed. Engl.* **2014**, *53*, 11935.
[39] P. Yang, P. Sun, L. Du, Z. Liang, W. Xie, X. Cai, L. Huang, S. Tan, W. Mai, *J. Phys. Chem. C* **2015**, *119*, 16483.
[40] P. Yang, P. Sun, W. Mai, *Mater. Today* **2016**, *19*, 394.
[41] N. Yoshida, Y. Yamada, S.-i. Nishimura, Y. Oba, M. Ohnuma, A. Yamada, *J. Phys. Chem. C* **2013**, *117*, 12003.
[42] C. Zhan, D. E. Jiang, *J. Phys. Condens. Matter* **2016**, *28*, 464004.
[43] C. Zhan, M. Naguib, M. Lukatskaya, P. R. C. Kent, Y. Gogotsi, D. E. Jiang, *J. Phys. Chem. Lett.* **2018**, *9*, 1223.
[44] Y.-P. Zhu, C. Xia, Y. Lei, N. Singh, U. Schwingenschlögl, H. N. Alshareef, *Nano Energy* **2019**, *56*, 357.
[45] S. Deebansok, J. Deng, E. Le Calvez, Y. Zhu, O. Crosnier, T. Brousse, O. Fontaine, *Nat. Commun.* **2024**, *15*, 1133.
[46] J. Wang, J. Polleux, J. Lim, B. Dunn, *J. Phys. Chem. C* **2007**, *111*, 14925.
[47] C. Costentin, *J. Phys. Chem. Lett.* **2020**, *11*, 9846.
[48] M. Forghani, S. W. Donne, *J. Electrochem. Soc.* **2018**, *165*, A664.
[49] G. Z. Chen, *Prog. Nat. Sci.: Mater. Int.* **2021**, *31*, 792.
[50] J. Bhagwan, N. Kumar, K. L. Yadav, Y. Sharma, *Solid State Ionics* **2018**, *321*, 75.
[51] A. Blidberg, T. Gustafsson, C. Tengstedt, F. Björefors, W. R. Brant, *Chem. Mater.* **2017**, *29*, 7159.
[52] Z. Chen, F. Xu, S. Cao, Z. Li, H. Yang, X. Ai, Y. Cao, *Small* **2017**, *13*, 1603148.
[53] R. Dong, Q. Ye, L. Kuang, X. Lu, Y. Zhang, X. Zhang, G. Tan, Y. Wen, F. Wang, *ACS Appl. Mater. Interfaces* **2013**, *5*, 9508.
[54] O. A. Drozhzhin, I. V. Tertov, A. M. Alekseeva, D. A. Aksyonov, K. J. Stevenson, A. M. Abakumov, E. V. Antipov, *Chem. Mater.* **2019**, *31*, 7463.
[55] J. Du, L. Jiao, Q. Wu, Y. Liu, Y. Zhao, L. Guo, Y. Wang, H. Yuan, *Electrochim. Acta* **2013**, *103*, 219.
[56] X. Geng, Y. Zhang, Y. Han, J. Li, L. Yang, M. Benamara, L. Chen, H. Zhu, *Nano Lett.* **2017**, *17*, 1825.
[57] E. Goikolea, B. Daffos, P. L. Taberna, P. Simon, *Mater. Renewable Sustainable Energy* **2013**, *2*, 16.
[58] D. Guo, H. Zhang, X. Yu, M. Zhang, P. Zhang, Q. Li, T. Wang, *J. Mater. Chem. A* **2013**, *1*, 7247.
[59] D. He, T. Wu, B. Wang, Y. Yang, S. Zhao, J. Wang, H. Yu, *Chem. Commun. (Cambridge, U. K.)* **2019**, *55*, 2234.
[60] A. I. Inamdar, A. T. A. Ahmed, H. S. Chavan, Y. Jo, S. Cho, J. Kim, S. M. Pawar, B. Hou, S. Cha, H. Kim, H. Im, *Ceram. Int.* **2018**, *44*, 18625.
[61] H. Jang, W. Jin, G. Nam, Y. Yoo, J. S. Jeon, J. Park, M. G. Kim, J. Cho, *Energy Environ. Sci.* **2020**, *13*, 2167.
[62] T. Jenkins, J. A. Alarco, I. D. R. Mackinnon, *ACS Omega* **2021**, *6*, 1917.
[63] J. W. Kim, V. Augustyn, B. Dunn, *Adv. Energy Mater.* **2012**, *2*, 141.
[64] N. H. Kwon, H. Yin, T. Vavrova, J. H. W. Lim, U. Steiner, B. Grobéty, K. M. Fromm, *J. Power Sources* **2017**, *342*, 231.
[65] J. Lu, H. Ran, J. Li, J. Wan, C. Wang, P. Ji, X. Wang, G. Liu, C. Hu, *Electrochim. Acta* **2020**, *331*, 135426.
[66] X. Lu, M. Yu, T. Zhai, G. Wang, S. Xie, T. Liu, C. Liang, Y. Tong, Y. Li, *Nano Lett.* **2013**, *13*, 2628.
[67] M. R. Lukatskaya, O. Mashtalir, C. E. Ren, Y. Dall'agnese, P. Rozier, P. L. Taberna, M. Naguib, P. Simon, M. W. Barsoum, Y. Gogotsi, *Science* **2013**, *341*, 1502.
[68] K. Malaie, F. Scholz, *Colloids Surf., A* **2019**, *577*, 576.
[69] J. Mu, J. Wang, J. Hao, P. Cao, S. Zhao, W. Zeng, B. Miao, S. Xu, *Ceram. Int.* **2015**, *41*, 12626.
[70] V. D. Nithya, K. Pandi, Y. S. Lee, R. K. Selvan, *Electrochim. Acta* **2015**, *167*, 97.
[71] M. Opitz, J. Yue, J. Wallauer, B. Smarsly, B. Roling, *Electrochim. Acta* **2015**, *168*, 125.
[72] L. Qu, Y. Liu, S. Fang, L. Yang, S.-i. Hirano, *Electrochim. Acta* **2015**, *163*, 123.
[73] R. B. Rakhi, B. Ahmed, M. N. Hedhili, D. H. Anjum, H. N. Alshareef, *Chem. Mater.* **2015**, *27*, 5314.
[74] R. B. Rakhi, W. Chen, D. Cha, H. N. Alshareef, *Nano Lett.* **2012**, *12*, 2559.
[75] S. Sahoo, S. Ratha, C. S. Rout, *Am. J. Eng. Appl. Sci.* **2015**, *8*, 371.
[76] P. M. Shafi, N. Joseph, A. Thirumurugan, A. C. Bose, *Chem. Eng. J.* **2018**, *338*, 147.
[77] Q. Shan, X. Mu, M. Alhabeb, C. E. Shuck, D. Pang, X. Zhao, X.-F. Chu, Y. Wei, F. Du, G. Chen, Y. Gogotsi, Y. Gao, Y. Dall'Agnese, *Electrochem. Commun.* **2018**, *96*, 103.
[78] L. Shen, S. Chen, J. Maier, Y. Yu, *Adv. Mater.* **2017**, *29*, 1701571.
[79] P. Singh, K. Shiva, H. Celio, J. B. Goodenough, Eldfellite, *Energy Environ. Sci.* **2015**, *8*, 3000.
[80] S. V. P. Vattikuti, K. C. Devarayapalli, N. N. Dang, J. Shim, *Ceram. Int.* **2021**, *47*, 11602.
[81] V. Vignesh, K. Subramani, M. Sathish, R. Navamathavan, *Colloids Surf., A* **2018**, *538*, 668.
[82] R. C. Vincent, P. Vishnoi, M. B. Preefer, J. X. Shen, F. Seeler, K. A. Persson, R. Seshadri, *ACS Appl. Mater. Interfaces* **2020**, *12*, 48662.
[83] M. Vujković, M. Mitrić, S. Mentus, *J. Power Sources* **2015**, *288*, 176.
[84] D. Wang, J. Xiao, W. Xu, Z. Nie, C. Wang, G. Graff, J.-G. Zhang, *J. Power Sources* **2011**, *196*, 2241.
[85] J. M. Whiteley, S. Hafner, S. S. Han, S. C. Kim, V.-D. Le, C. Ban, Y. H. Kim, K. H. Oh, S.-H. Lee, *J. Mater. Chem. A* **2017**, *5*, 15661.
[86] C. Wu, Z. G. Wu, X. Zhang, R. Rajagopalan, B. Zhong, W. Xiang, M. Chen, H. Li, T. Chen, E. Wang, Z. Yang, X. Guo, *ACS Appl. Mater. Interfaces* **2017**, *9*, 43596.
[87] J. Xiao, J. Wen, J. Zhao, X. Ma, H. Gao, X. Zhang, *Electrochim. Acta* **2020**, *337*, 135803.
[88] P. F. Xiao, M. O. Lai, L. Lu, *Solid State Ionics* **2013**, *242*, 10.
[89] H. Xu, J. Shu, X. Hu, Y. Sun, W. Luo, Y. Huang, *J. Mater. Chem. A* **2013**, *1*, 15053.
[90] W. Xu, Z. Jiang, Q. Yang, W. Huo, M. S. Javed, Y. Li, L. Huang, X. Gu, C. Hu, *Nano Energy* **2018**, *43*, 168.
[91] Y. Yang, L. Li, G. Ruan, H. Fei, C. Xiang, X. Fan, J. M. Tour, *ACS Nano* **2014**, *8*, 9622.
[92] J. Zhang, J. Ma, L. L. Zhang, P. Guo, J. Jiang, X. S. Zhao, *J. Phys. Chem. C* **2010**, *114*, 13608.
[93] Y. Zhang, Z. Ding, C. W. Foster, C. E. Banks, X. Qiu, X. Ji, *Adv. Funct. Mater.* **2017**, *27*, 1700856.
[94] G. Zhao, N. Zhang, K. Sun, *Mater. Res. Bull.* **2013**, *48*, 1328.
[95] J.-c. Zheng, Y.-d. Han, L.-b. Tang, B. Zhang, *Electrochim. Acta* **2016**, *198*, 195.
[96] H. Zhu, H. He, X. Xin, X. Ma, L. Zan, Y. Zhang, *Electrochim. Acta* **2015**, *155*, 116.
[97] J. W. Long, E. S. K., C. I. Merzbacher, D. R. Rolison, *Langmuir* **1999**, *15*, 780.
[98] W. Sugimoto, K. Yokoshima, Y. Murakami, Y. Takasu, *Electrochim. Acta* **2006**, *52*, 1742.
[99] B. Anasori, M. R. Lukatskaya, Y. Gogotsi, *Nat. Rev. Mater.* **2017**, *2*, 16098.
[100] M. Hu, H. Zhang, T. Hu, B. Fan, X. Wang, Z. Li, *Chem. Soc. Rev.* **2020**, *49*, 6666.
[101] J. Liu, J. Wang, Y. Ni, K. Zhang, F. Cheng, J. Chen, *Mater. Today* **2021**, *43*, 132.

[102] H.-J. Kim, T. N. V. Krishna, K. Zeb, V. Rajangam, C. V. V. M. Gopi, S. Sambasivam, K. V. G. Raghavendra, I. M. Obaidat, *Electronics* **2020**, *9*, 1161.
[103] V. Augustyn, P. Simon, B. Dunn, *Energy Environ. Sci.* **2014**, *7*, 1597.
[104] Y. Jiang, J. Liu, *Energy Environ. Mater.* **2019**, *2*, 30.
[105] C. Choi, D. S. Ashby, D. M. Butts, R. H. DeBlock, Q. Wei, J. Lau, B. Dunn, *Nat. Rev. Mater.* **2020**, *5*, 5.
[106] X. Li, Z. Huang, C. E. Shuck, G. Liang, Y. Gogotsi, C. Zhi, *Nat. Rev. Chem.* **2022**, *6*, 389.
[107] S. Fleischmann, Y. Zhang, X. Wang, P. T. Cummings, J. Wu, P. Simon, Y. Gogotsi, V. Presser, V. Augustyn, *Nat. Energy* **2022**, *7*, 222.
[108] S. B., G. Trasatti, *J. Electroanal. Chem.* **1971**, *29*, A1.
[109] R. A. Marcus, *J. Chem. Phys.* **1965**, *43*, 679.
[110] J. M. Savéant, *J. Phys. Chem. B* **2002**, *106*, 9387.
[111] D. Fraggedakis, M. McEldrew, R. B. Smith, Y. Krishnan, Y. Zhang, P. Bai, W. C. Chueh, Y. Shao-Horn, M. Z. Bazant, *Electrochim. Acta* **2021**, *367*, 137432.